

# 1 Isolating the Contributions of Specific Network Sites to the Diffuse 2 Vibrational Spectrum of Interfacial Water with Isotopomer-Selective 3 Spectroscopy of Cold Clusters

4 Nan Yang, Thien Khuu, Sayoni Mitra, Chinh H. Duong, Mark A. Johnson,\* Ryan J. DiRisio,  
5 Anne B. McCoy, Evangelos Miliordos, and Sotiris S. Xantheas



Cite This: <https://dx.doi.org/10.1021/acs.jpca.0c07795>



Read Online

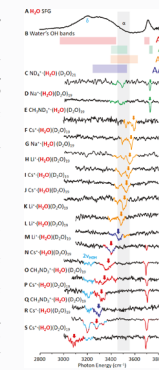
ACCESS |

Metrics & More

Article Recommendations

Supporting Information

6 **ABSTRACT:** Decoding the structural information contained in the interfacial vibrational spectrum of water  
7 requires understanding how the spectral signatures of individual water molecules respond to their local hydrogen  
8 bonding environments. In this study, we isolated the contributions for the five classes of sites that differ according  
9 to the number of donor (D) and acceptor (A) hydrogen bonds that characterize each site. These patterns were  
10 measured by exploiting the unique properties of the water cluster cage structures formed in the gas phase upon  
11 hydration of a series of cations  $M^+(H_2O)_n$  ( $M = Li, Na, Cs, NH_4, CH_3NH_3, H_3O$ , and  $n = 5, 20-22$ ). This  
12 selection of ions was chosen to systematically express the A, AD, AAD, ADD, and AADD hydrogen bonding motifs.  
13 The spectral signatures of each site were measured using two-color, IR–IR isotopomer-selective photo-  
14 fragmentation vibrational spectroscopy of the cryogenically cooled, mass selected clusters ions in which a single  
15 intact  $H_2O$  is introduced without isotopic scrambling, an important advantage afforded by the cluster regime. The  
16 resulting patterns provide an unprecedented picture of the intrinsic line shapes and spectral complexities associated  
17 with excitation of the individual OH groups, as well as the correlation between the frequencies of the two OH  
18 groups on the same water molecule, as a function of network site. The properties of the surrounding water network  
19 that govern this frequency map are evaluated by dissecting electronic structure calculations that explore how changes in the nearby  
20 network structures, both within and beyond the first hydration shell, affect the local frequency of an OH oscillator. The qualitative  
21 trends are recovered with a simple model that correlates the OH frequency with the network-modulated local electron density in the  
22 center of the OH bond.



## I. INTRODUCTION

23 The very large range (3000–3700  $cm^{-1}$ ) spanned by the OH  
24 stretching vibrational spectrum of liquid water reveals the wide  
25 distribution of intramolecular distortions caused by variations in  
26 the H-bonding topologies of the surrounding network. The  
27 distribution of OH frequencies has been considered in the  
28 context of the local electric fields that are present in particular  
29 binding sites, which in turn reflect the number of directly  
30 coordinated water molecules as well as the orientations of water  
31 molecules in the more distant hydration shells.<sup>1–4</sup> The variation  
32 in this coordination number is particularly relevant to the  
33 spectrum of the air–water interface, where there are many  
34 nonbonded OH groups. There is a consensus that the dominant  
35 interactions governing the local OH frequency are the number  
36 of H-bond donor (D) and acceptor (A) molecules attached to  
37 the water molecule in question.<sup>3–5</sup> The OH frequency  
38 distributions reported by Skinner and co-workers<sup>1,4</sup> for five  
39 classes of coordination environment (A, AD, AAD, ADD, and  
40 AADD) are reproduced in Figure 1 to illustrate the ranges of  
41 activity expected for each class. Note that within a coordination  
42 class, the distributions are very broad such that the red-shifted  
43 bands arising from the bound OH groups overlap, as do the  
44 fundamentals arising from the nonbonded OH groups near 3700  
45  $cm^{-1}$ . As such, the factors that govern the local frequency must

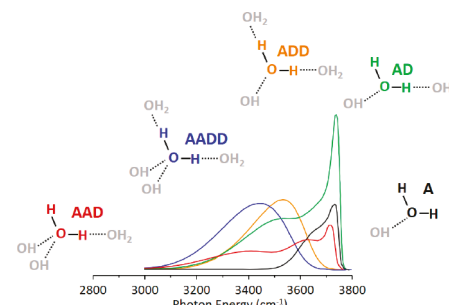


**Figure 1.** Color-coded frequency distributions of the two OH stretches arising from water molecules surrounded by various acceptor (A) and donor (D) H-bonding arrangements. Reproduced from ref 4 with permission. Copyright 2015 AIP.

Received: August 26, 2020

Revised: October 26, 2020

reflect different topologies of the water network beyond the first shell. Consequently, both Skinner<sup>5</sup> and Ohno<sup>3</sup> have advanced more elaborate schemes that take into account the coordination environments of the water molecules that are attached to the molecule whose frequency is under consideration. Although the simulations provide a compelling microscopic picture of how different structures contribute to the spectrum, experimental verification of these predicted contributions presents a profound challenge. For example, recent efforts to directly extract the contribution from the  $3500\text{ cm}^{-1}$  region using surface-sensitive spectroscopies yielded different spectral responses, pointing to the complexities of isolating the ambient (as opposed to laser-driven) contributions to the linear spectrum.<sup>6,7</sup>

Very recently, the unique advantages of cryogenic, gas phase cluster spectroscopy<sup>8,9</sup> have proven useful to disentangle the contributions of the AAD and ADD sites using the  $\text{Cs}^+(\text{H}_2\text{O})_{20}$  cluster as a model system.<sup>10</sup> This system adopts a clathrate cage structure constructed from 12 interlocking, cyclic water pentamers (a pentagonal dodecahedron, PD). The advantage of the PD structure is that it only has AAD and ADD sites, thus eliminating congestion from other sites. Importantly, the OH stretching spectrum of  $\text{Cs}^+(\text{H}_2\text{O})_{20}$  is still diffuse, spanning the range displayed by the air–water interface (see Figure 2E). This occurs despite the fact that only two sites are in play because the network topologies are quite diverse with respect to the H-bond configurations in the surrounding hydration shells, with the result that the bound OH (hereafter  $\text{OH}^b$ ) contributions occur over hundreds of wavenumbers. Nonetheless, these overlapping contributions could be completely disentangled by leveraging cluster regime suppression of H/D isotopic exchange.<sup>11,12</sup> This allows the incorporation of a single, intact  $\text{H}_2\text{O}$  molecule into an otherwise perdeuterated water cage. The labeled water was observed to statistically occupy all spectroscopically distinct sites, creating an isotopologue that is a heterogeneous ensemble of isotopomers that differ according to the site occupied by the isotopic label. The vibrational spectrum of each isotopomer can then be isolated experimentally using two-color, IR–IR photobleaching techniques routinely used in ion photodissociation spectroscopy to separate the spectra of structural isomers.<sup>8</sup> Importantly, because there is only one  $\text{H}_2\text{O}$  molecule in any given cluster, the spectrum of each isotopomer consists of the correlated absorptions of its two OH groups and any “extra” features arising from anharmonicities.<sup>8,13</sup> We herein present the results of similar site-specific measurements on a series of water clusters where both cluster size and guest cation are varied systematically to reveal the spectral signatures of all the sites that are relevant to the deconstruction of the interfacial IR spectrum. The particular systems selected to accomplish this goal are indicated in Figure 2C–G along with their vibrational spectra obtained by IR photodissociation of a weakly bound  $\text{D}_2$  molecule. The sum of these spectra (Figure 2B) is compared to the surface-selective (sum frequency generation, SFG) spectrum of the water interface<sup>14–16</sup> (Figure 2A) to confirm, that taken together, the cluster systems span the same frequency range. Note that the selection rules for SFG are different from those of the linear absorption regime at play in the cluster spectra and differences in shape are expected.<sup>1,4</sup> We consider the site-specific contributions to this broad envelope in the context of qualitative rules of H-bonding commonly invoked to deconstruct the spectrum of the air–water interface. We also caution that the behavior of a single water molecule in a perdeuterated environment suppresses intermolecular coupling at play at the bulk interface of homogeneous  $\text{H}_2\text{O}(l)$ .

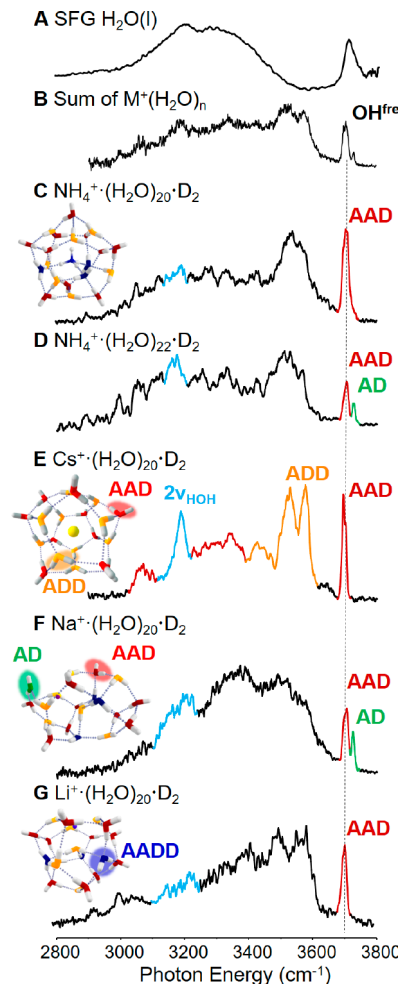


**Figure 2.** SFG spectrum of the air–water interface compared to the spectra of various water clusters in the OH region. (A) SFG intensity ( $\chi^{(2)p}$ ) spectrum. Reproduced from ref 15 with permission.  $\delta$  denotes the bend overtone ( $2\nu_{\text{HOH}}$ ) transition, and  $\alpha$  denotes the controversial region around  $3500\text{ cm}^{-1}$ . (B) Sum of cluster spectra in (C)–(G) weighted equally by peak area.  $\text{D}_2$ -tagged predissociation spectra and representative structures of (C)  $\text{NH}_4^+(\text{H}_2\text{O})_{20}$ , (D)  $\text{NH}_4^+(\text{H}_2\text{O})_{22}$ , (E)  $\text{Cs}^+(\text{H}_2\text{O})_{20}$ , (F)  $\text{Na}^+(\text{H}_2\text{O})_{20}$ , and (G)  $\text{Li}^+(\text{H}_2\text{O})_{20}$ .<sup>19</sup> OH stretching bands and water molecules in the structures are color-coded according to their types.

Nonetheless, these patterns provide an unprecedented view into how local structures contribute to various regions of the OH stretching spectrum.

## II. RESULTS AND DISCUSSION

**II.A. Dependence of Water Network Structures and H-Bonding Site Types on Cation and Size.** The calculated structures for the cluster scaffolds used for this study are depicted in the insets in Figure 2C–G with the various sites highlighted in color. Rotatable pdf images are included in the Supporting Information. Note that the cluster structures in the  $n \sim 20$  size range adopt many thousands of isomeric forms that have similar oxygen atom frameworks but differ according to the orientations and topologies of the H-bonds that connect them.<sup>17</sup> These isomers are close in energy and are undoubtedly present under our experimental conditions, hence providing a large variation in local H-bond environments that contribute to the signal at any given frequency. As such, the ensemble of  $\sim 10\,000$

125 ions interrogated in these measurements resembles the diverse  
126 environments experienced by interfacial water molecules in  
127 liquid or amorphous ice.

128 The changes in the cage structure with the size of the ion are  
129 reflected in the structures of the  $\text{Li}^+$ ,  $\text{Na}^+$ , and  $\text{Cs}^+$  clusters with  
130 20 water molecules. The  $\text{Na}^+(\text{H}_2\text{O})_{20}$  structure (Figure 2F)  
131 features a partial collapse of the PD cage present in the  $\text{Cs}^+$ .  
132  $(\text{H}_2\text{O})_{20}$  system (Figure 2E) as the  $\text{Na}^+$  ion migrates toward the  
133 surface, while the  $\text{Li}^+$  ion is accommodated at the surface in  $\text{Li}^+$ .  
134  $(\text{H}_2\text{O})_{20}$  (Figure 2G).<sup>18,19</sup> The ammonium ion, on the other  
135 hand, resides in the center of the  $(\text{H}_2\text{O})_{20}$  cluster but puckers the  
136 cage due to strong, directional interactions between  $\text{H}_2\text{O}$  and  
137  $\text{NH}_4^+$  as indicated in Figure 2C.<sup>20</sup> Table S1 presents a summary  
138 of the number of each site types predicted for calculated  
139 structures of the various systems used in the this work.

140 The spectra in Figure 2 illustrate how a specific  $\text{H}_2\text{O}$  bonding  
141 site can be introduced into the network by varying both ion  
142 identity and cluster size. For example, the distorted  $\text{Na}^+$ .  
143  $(\text{H}_2\text{O})_{20}$  system displays the telltale AD band (weaker member  
144 of the doublet in the  $\text{OH}^{\text{free}}$  stretching region highlighted in  
145 green), while the more symmetrical cage  $\text{Cs}^+(\text{H}_2\text{O})_{20}$  does not  
146 (compare Figure 2E,F). Although the AD peak is missing in the  
147  $\text{NH}_4^+(\text{H}_2\text{O})_{20}$  spectrum (Figure 2C), it is present upon  
148 addition of two water molecules in the  $n = 22$  cluster (green  
149 shoulder in Figure 2D). The spectral signatures of these AD  
150 binding sites can thus be isolated because the  $\text{OH}_{\text{AD}}^{\text{free}}$  band arising  
151 from this motif is clearly resolved between the free OH feature of  
152 the AAD molecules and the asymmetric stretch of water  
153 molecules in the A sites.<sup>21</sup> The latter are known from their  
154 positions in smaller cluster spectra with the sharp bands from  
155  $\text{H}_3\text{O}^+(\text{H}_2\text{O})_5$  displayed in Figure 4E, consistent with the  
156 simulated frequency distribution of this site on the interface in  
157 Figure 1 (black trace).<sup>1,22</sup> We note that the absence of this  
158  $\text{OH}_{\text{AD}}^{\text{free}}$  feature was key to the identification of the PD structures  
159 of  $\text{Cs}^+(\text{H}_2\text{O})_{20}$  and  $\text{H}_3\text{O}^+(\text{H}_2\text{O})_{20}$ ,<sup>23,24</sup> and the emergence of  
160 the AD feature in the  $\text{Cs}^+(\text{H}_2\text{O})_{20}$  spectrum at elevated  
161 temperature (200 K) has been recently exploited as a probe for  
162 the breakup of the PD cage.<sup>25</sup> On the other hand, isolation of the  
163 AADD site is the most challenging to achieve in the cluster  
164 systems because its features are expected to overlap with those  
165 from  $\text{OH}_{\text{AAD}}$  (Figure 1). The AADD sites are present in the  $n \sim$   
166 20 range in systems that accommodate the ions on the surface of  
167 the cage. This is the case in the  $\text{H}_3\text{O}^+(\text{H}_2\text{O})_{20}$  structure, for  
168 example, which features 5 AADD sites.<sup>26</sup> Unfortunately, it is not  
169 possible to incorporate an intact  $\text{H}_2\text{O}$  molecule in the  $\text{D}_3\text{O}^+$ .  
170  $(\text{D}_2\text{O})_{20}$  structure due to fast H/D exchange, but the  
171 hydrophobic methyl group in the  $\text{CH}_3\text{NH}_3^+$  ion also forces  
172 surface hydration in the  $\text{CH}_3\text{NH}_3^+(\text{H}_2\text{O})_{20}$  system. That  
173 system is also calculated to accommodate 5 molecules in  
174 AADD sites (see Table S1), but importantly does not exhibit H/  
175 D exchange because of the increased basicity of the amine group,  
176 and hence was chosen for this study. To gauge the extent of the  
177 spectral coverage afforded by our choice of cluster systems,  
178 Figure 3 presents histograms of the calculated harmonic spectra,  
179 sorted and color coded by site type. We emphasize that this  
180 indicates the range of behaviors exhibited by specific structure  
181 types. It is expected that many more isomers are generated in the  
182 ion source and thus provide an even more complete sampling of  
183 the environments available to water molecules embedded in an  
184 extended network.

185 Because the cages are mostly composed of heavy water  
186 molecules, there is a possibility that nuclear quantum effects  
187 could induce changes in the specific cage structures.<sup>27,28</sup> To

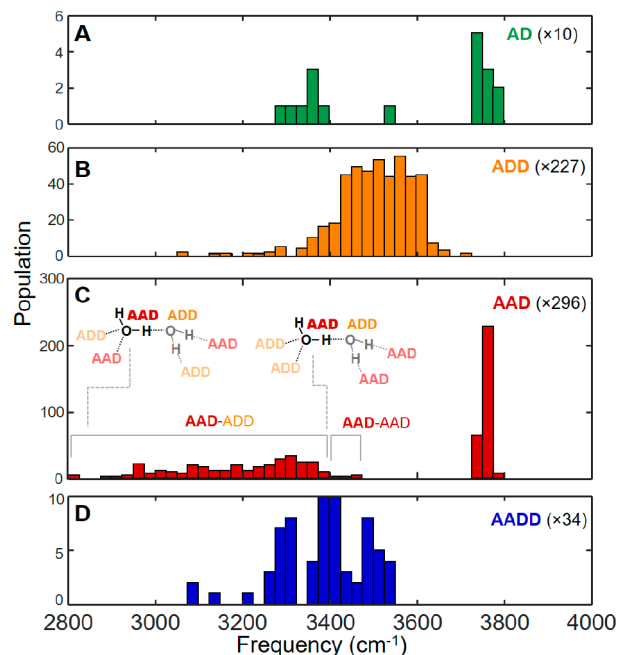
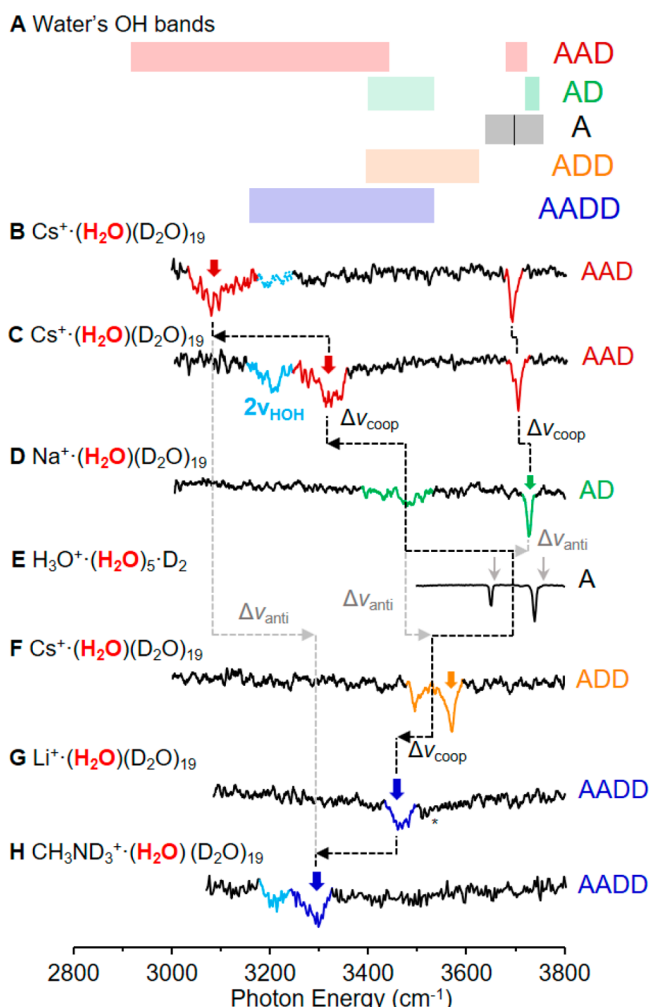


Figure 3. Calculated harmonic frequency distribution of various isomers of the  $\text{M}^+(\text{H}_2\text{O})(\text{D}_2\text{O})_{n-1}$  ( $\text{M} = \text{Li}, \text{Na}, \text{Cs}, \text{NH}_4^+, \text{CH}_3\text{NH}_3^+, \text{H}_3\text{O}^+$ , and  $n = 20-22$ ) clusters. The calculations were done at the B3LYP/6-31++G\*\* level of theory and basis set with the LANL2DZ pseudopotential for Cs and scaled by 0.973. The numbers near the A/D labels are the total number of water molecules shown in the panel. The bound OHs in panel C are classified according to the binding site types of the OH group of interest and its surrounding water molecules.

address this point, we compared the spectra of  $\text{M}^+(\text{H}_2\text{O})-(\text{D}_2\text{O})_{n-1}$  with those of  $\text{M}^+(\text{H}_2\text{O})_n$  for  $\text{M} = \text{Cs}, \text{Li}$ , and  $\text{Na}$  in Figure S2. In general, the band positions and envelopes are quite similar, indicating that the same structural class is present in both isotopologues.

**II.B. Survey of the Site-Dependent Spectral Patterns** Displayed by a Single  $\text{H}_2\text{O}$  Molecule Embedded in Three-Dimensional H-Bonded Cages. Isotopomer-selective spectra were obtained using a two-color, IR-IR photobleaching variation in triple-focusing photofragmentation mass spectrometry (IR<sup>2</sup>MS<sup>3</sup>) described in detail in ref 8. Briefly, a particular isotopomer with composition  $\text{M}^+(\text{H}_2\text{O})(\text{D}_2\text{O})_n$  is selected for interaction with a probe laser with its frequency fixed on a transition associated with one of its isotopomers. The photofragment from the probe laser is monitored continuously to record the population in the isotopomer selected according to the carrier of the band to which it is tuned. Prior to this interaction, a powerful photobleaching laser intercepts the same ion packet and removes the population of each isotopomer as it is scanned across the entire spectrum. Hence all bands associated with the two OH groups on the site occupied by the single  $\text{H}_2\text{O}$  molecule then appear as downward going features (dips) according to the population depletions driven by the bleach laser.

Figure 4 presents a summary of a large data set collected using the six cations and various water cluster sizes, which were selected to illustrate the different (persistent) patterns associated with the various site types. The entire set is included in Figure S1. These patterns were obtained by scanning the bleach laser while fixing a probe laser at the locations of the downward arrows. The most difficult site to reveal is the AADD because it does not have a unique spectral feature in the high



**Figure 4.** Frequency ranges of the various binding sites available to water molecules at the interface, with representative spectral patterns displayed by a single  $\text{H}_2\text{O}$  molecule embedded in each site. (A) Frequency ranges displayed by a single  $\text{H}_2\text{O}$  molecule embedded in  $\text{D}_2\text{O}$  clusters in various combinations of acceptor “A” and donor “D” H-bonding environments. The black vertical line in the gray box denotes the decoupled local free OH stretch in an acceptor water molecule. (B)–(H) Representative patterns of the spectral signatures of the sites obtained from isotopomer-specific spectra of (B, C, F)  $\text{Cs}^+(\text{H}_2\text{O})\cdot(\text{D}_2\text{O})_{19}$ , (D)  $\text{Na}^+(\text{H}_2\text{O})\cdot(\text{D}_2\text{O})_{19}$ , (E)  $\text{H}_3\text{O}^+(\text{H}_2\text{O})_5$ , (G)  $\text{Li}^+(\text{H}_2\text{O})\cdot(\text{D}_2\text{O})_{19}$ , and (H)  $\text{CH}_3\text{ND}_3^+(\text{H}_2\text{O})\cdot(\text{D}_2\text{O})_{19}$ . The OH stretching bands are color-coded according to their site types in (A). The complete set of spectra is included in Figure S1.  $2\nu_{\text{HOH}}$  denotes the bend overtone, while  $\Delta\nu_{\text{coop}}$  and  $\Delta\nu_{\text{anti}}$  labels on arrows denotes the frequency shifts caused by cooperative and anticooperative interactions displayed by adding a second H-bond to an open coordination site.

patterns (compared to the complex spectra of the homogeneous isotopomers in Figure 2) is important because it demonstrates that the spectral signatures of the embedded water molecules are not complicated by the presence of combination bands with soft modes. Such complications are known to arise from surprisingly strong electrical and mechanical anharmonicities in smaller water cluster ion systems.<sup>8,30–32</sup> The widths of the bands, on the other hand, appear to systematically increase with the red shift, an effect noted earlier in the case of the isolated OH groups in spectra obtained by incorporation of a single HOD molecule in the 20 water molecule cages.<sup>33</sup>

The site-specific band patterns (Figure 4) provide a remarkably clear picture of how the local H-bonding configuration drives the qualitative trends in the embedded band patterns (Figure 1). We begin with the simple doublet pattern associated a single acceptor water molecule (“A” in Figure 1) attached to an OH group such that both of its OH groups are free (Figure 4E). These two bands are the fundamentals of the symmetric ( $\nu_{\text{sym}}$ ) and antisymmetric ( $\nu_{\text{asym}}$ ) OH stretching normal modes, which lie very close to the origins of those found in the bare water molecule (gray downward arrows in Figure 4E). If one adopts a local OH mode perspective, the  $\sim 100 \text{ cm}^{-1}$  spacing between these bands can be viewed as the coupling matrix element between the degenerate OH groups. Interestingly, when the A motif reorients into the surface to donate two H-bonds and adopt the ADD environment, the doublet pattern (Figure 4F) retains the  $\sim 2/1$  intensity ratio with about 20% contraction of the splitting, while the centroid red shifts by about  $200 \text{ cm}^{-1}$  (Figure 4E,F). This red shift is further increased upon accepting another H-bond to form the AADD (Figure 4G,H), which is the behavior expected for cooperative H-bonding in which accepting a second H-bond enhances the first. Notice, however, that the broad  $\text{OH}_{\text{AADD}}^{\text{b}}$  feature does not appear as a doublet, suggesting that the second acceptor H-bond suppresses the coupling between the OH groups. Interestingly, Skinner and co-workers<sup>34</sup> considered this intramolecular coupling in simulations of condensed phase water and ice and concluded that the coupling matrix element is indeed reduced in the fully coordinated environment. Although the signal-to-noise in the AADD spectra is somewhat degraded, the trace in Figure 4H suggests that the Fermi resonance with the bend overtone is retained, a provocative observation that warrants further investigation beyond the scope of this work.

The traces progressing upward from Figure 4E display the trends associated with retention of one free OH group while donating an H-bond with its partner OH group, and sequentially adding acceptor groups. The formation of one donor bond to the A site creates the AD site (Figure 4D), which results in a  $\sim 200 \text{ cm}^{-1}$  red shift in the  $\text{OH}_{\text{AD}}^{\text{b}}$  stretch as expected. Note that the  $\text{OH}_{\text{AD}}^{\text{free}}$  band also red-shifts and moves toward the  $3705 \text{ cm}^{-1}$  centroid of the normal modes in a free water molecule (the same frequency as the OH stretch in isolated HOD).<sup>35</sup> The latter shift occurs because the coupling between the two groups is suppressed when the separation between the two bands is significantly larger than the intrinsic coupling matrix element ( $\sim 50 \text{ cm}^{-1}$ ). Although the red-shifted  $\text{OH}_{\text{AD}}^{\text{b}}$  fundamental is broadened (from 10 to  $35 \text{ cm}^{-1}$ ) in keeping with expected H-bond behavior, it does not exhibit the intensity enhancement that is typical for H-bonds in binary systems.<sup>36</sup> When the AD site accepts another bond to form the AAD site, the  $\text{OH}_{\text{AAD}}^{\text{free}}$  transition falls closer to the decoupled OH stretch in HOD, and its companion  $\text{OH}_{\text{AAD}}^{\text{b}}$  transition further red-shifts by 200–

220 energy region, and the samples presented in Figure 4H required 221 deconvolution as described in detail in section SII of the 222 Supporting Information.

223 An interesting feature of the patterns displayed in Figure 4 is 224 that they are quite simple, mostly consisting of two features as 225 would be expected for the two OH stretching fundamentals on a 226 water molecule at the harmonic level. The only exception is the 227 “extra” band (turquoise in Figure 4C,H) that appears around 228  $3200 \text{ cm}^{-1}$ . This feature arises from a Fermi-resonance 229 interaction between the overtone of the HOH bending mode 230 and OH stretching fundamentals that are red-shifted into 231 resonance with the bend overtone.<sup>10,29</sup> The simplicity of these

294  $400\text{ cm}^{-1}$  ( $\Delta\nu_{\text{coop}}$  in Figure 4C,D) as it broadens and gains  
295 intensity.

296 Finally, the survey in Figure 4 also reveals the consequence of  
297 converting an AD site (Figure 4D) into an ADD site (Figure 4F)  
298 by forming a second donor bond. This **blue-shifts**  $\nu_{\text{AD}}^{\text{b}}$  by about  
299  $50\text{ cm}^{-1}$  ( $\Delta\nu_{\text{anti}}$  between Figure 4D,F) toward the centroid of  
300 the doublet in the  $\text{OH}_{\text{ADD}}^{\text{b}}$  pattern, indicating a weakening or  
301 anticooperative interaction between the two bound OH groups.  
302 A similar effect is observed in the case of transforming AAD into  
303 AADD (Figure 4B,H).

304 **II.C. Frequency Ranges Explored by the A, AD, ADD,  
305 and AAD Sites.** Figure 5 compares the frequency ranges  
306 associated with each binding class, which are displayed along  
307 with the predicted contributions to the spectrum of the air-

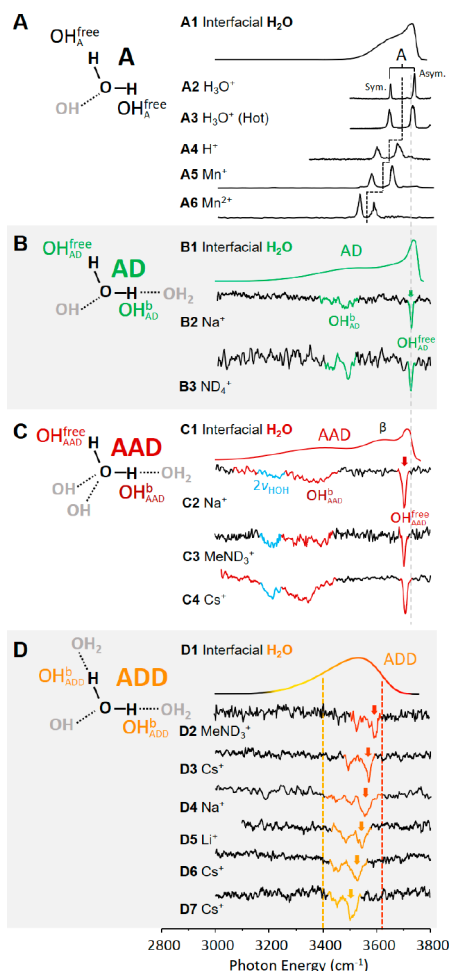


**Figure 5.** Calculated OH frequency distribution of water molecules classified by their H-bond environment at the air water interface compared to spectra obtained with finite size water clusters of the corresponding sites. Example structures, calculated frequency distributions (ref 4, upward traces), and experimental spectra (downward traces) from various water clusters of single acceptor (A), acceptor-donor (B), acceptor-acceptor-donor (C), and acceptor-donor-donor (D) water molecules. The spectra are color coded according to the water molecule's acceptor donor type. Spectra from specific clusters are presented in (A2)  $\text{H}_3\text{O}^{\cdot}\cdot(\text{H}_2\text{O})_5$ , (A3)  $\text{H}_3\text{O}^{\cdot}\cdot(\text{H}_2\text{O})_3$ , (A4)  $\text{H}^{\cdot}\cdot(\text{H}_2\text{O})_2$ , (A5)  $\text{Mn}^{\cdot}\cdot(\text{H}_2\text{O})$ , (A6)  $\text{Mn}^{2+}\cdot(\text{H}_2\text{O})$ , and (B3)  $\text{ND}_4^{\cdot}\cdot(\text{H}_2\text{O})\cdot(\text{D}_2\text{O})_{21}$ . The rest have the  $\text{M}^{\cdot}$  labels correspond to the cation in a  $\text{M}^{\cdot}\cdot(\text{H}_2\text{O})\cdot(\text{D}_2\text{O})_{19}$ , for example, (B2) would be  $\text{Na}^{\cdot}\cdot(\text{H}_2\text{O})\cdot(\text{D}_2\text{O})_{19}$ . (A5, A6) are reproduced from ref 35 with permission.

water interface (solid curves above experimental spectra in Figure 5).<sup>1,22</sup>

The frequency range displayed by the A sites is readily available because the  $\nu_{\text{sym}}$  and  $\nu_{\text{asym}}$  bands are easily identified in the linear absorption spectrum. To sample the range available to the A sites, however, we note that these only occur in minimum energy structures at smaller cluster sizes. In general, the free OH frequency has been correlated with the local electric field at the surface,<sup>36–38</sup> such that the centroid of the  $\nu_{\text{sym}}$  and  $\nu_{\text{asym}}$  doublet **red-shifts** as the two bands come closer together. Several examples demonstrating this effect are included in Figure 5A in which  $\text{H}_2\text{O}$  is attached to a water molecule, a hydronium ion, a proton,  $\text{Mn}^+$  and  $\text{Mn}^{2+}$  (Figure 5A2–A6, respectively).<sup>37</sup> Note that the intensity of the two bands also inverts in a strong electric field such that the lower energy  $\nu_{\text{sym}}$  band is dominant upon attachment to a +2 charged ion. The calculated range at the interface samples much of this range but likely does so because of large amplitude dispacements driven by thermal fluctuations, which bring the nominally free OH groups closer to H-bond acceptors on the surface. Part of this effect can also be simulated using clusters warmed by absorption of a IR photon, leading to the broadened feature displayed in Figure 5A3.

The frequency ranges explored by the bound  $\text{OH}_{\text{AD}}^{\text{b}}$  and  $\text{OH}_{\text{AAD}}^{\text{b}}$  oscillators can be unambiguously determined using  $\text{IR}^2\text{MS}^3$  spectroscopy in a mode where the probe laser is tuned to one of the well-resolved free partner oscillators ( $\text{OH}_{\text{AD}}^{\text{free}}$  and  $\text{OH}_{\text{AAD}}^{\text{free}}$ ), highlighted in green and red in Figure 2, respectively. Specifically, by setting the probe laser on one of these bands, the locations of all of the absorptions arising from the bound OH groups within each class,  $\text{OH}_{\text{AD}}^{\text{b}}$  and  $\text{OH}_{\text{AAD}}^{\text{b}}$ , are revealed by scanning the bleach laser through the spectrum. The  $\text{OH}_{\text{AD}}^{\text{b}}$  bands were obtained by applying the  $\text{IR}^2\text{MS}^3$  method to the  $\text{ND}_4^{\cdot}\cdot(\text{H}_2\text{O})\cdot(\text{D}_2\text{O})_{21}$  and  $\text{Na}^{\cdot}\cdot(\text{H}_2\text{O})\cdot(\text{D}_2\text{O})_{19}$  clusters. Both systems yield  $\text{OH}_{\text{AD}}^{\text{b}}$  activity over a narrow ( $\sim 100\text{ cm}^{-1}$ ) range near  $3500\text{ cm}^{-1}$ , consistent with the simulated contributions from AD molecules displayed in Figure 5B1.

In contrast to the AD behavior, the  $\text{OH}_{\text{AAD}}^{\text{b}}$  contributions span a larger range from  $3100$  to  $3450\text{ cm}^{-1}$ . Note that the  $\text{Na}^{\cdot}\cdot(\text{H}_2\text{O})\cdot(\text{D}_2\text{O})_{19}$  system exhibits both AAD and AD sites so that the different behaviors are displayed by the same cluster. In addition, the range of its  $\text{OH}_{\text{AAD}}^{\text{b}}$  envelope, as well as that displayed by  $\text{CH}_3\text{ND}_3^{\cdot}\cdot(\text{H}_2\text{O})\cdot(\text{D}_2\text{O})_{19}$ , are similar to that found in the more symmetrical  $\text{Cs}^{\cdot}\cdot(\text{H}_2\text{O})\cdot(\text{D}_2\text{O})_{19}$  system but extend to slightly higher energy (by  $\sim 50\text{ cm}^{-1}$ ). We emphasize that the  $\text{OH}_{\text{AAD}}^{\text{b}}$  envelope has been deconstructed to reveal the heterogeneity of the broad envelope in the  $\text{Cs}^{\cdot}$  system, with two examples presented in Figure 4. A more complete set of these patterns is presented in Figure S1, which illustrates how the  $\text{OH}_{\text{AAD}}^{\text{b}}$  broadens and effectively “tunes” through the Fermi resonance with the bend overtone with the increasing **red shift**. The observed  $\text{OH}_{\text{AAD}}^{\text{b}}$  behavior is not consistent with that calculated (Figure 5C1),<sup>1,4</sup> however, as there is no observed activity in the region of the higher energy shoulder predicted near  $3600\text{ cm}^{-1}$  (labeled  $\beta$  in Figure 5C). This discrepancy may reflect the fact that at  $300\text{ K}$ , the large amplitude motions in the liquid enhance the contributions from more open structures while the cold clusters correspond to the intrinsic behavior of the local minima.

It is more difficult to determine the spectral range of the ADD sites because they do not have a feature common to all of the variations available in the clusters, as do the A and AD sites. Nonetheless, the range in the patterns could be established by probing many frequencies in the  $3400$ – $3600\text{ cm}^{-1}$  region where

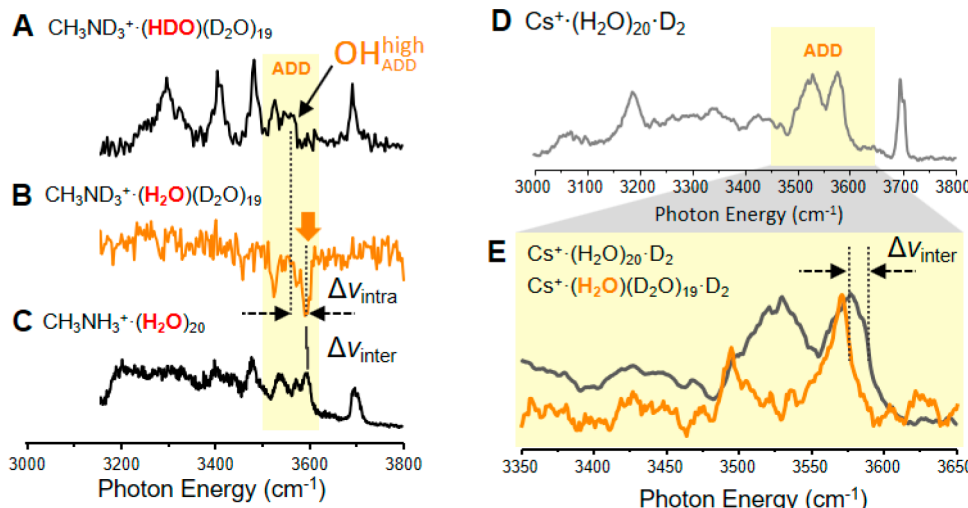


**Figure 6.** Experimental spectra illustrating the frequency shift caused by intra- and intermolecular coupling. (A) vibrational predissociation spectrum of  $\text{CH}_3\text{ND}_3^+\cdot(\text{HDO})(\text{D}_2\text{O})_{19}$ . The  $\text{OH}_{\text{ADD}}^{\text{high}}$  labels the highest energy OH feature arising from ADD water molecules. (B) isotopomer-specific spectra of  $\text{CH}_3\text{ND}_3^+\cdot(\text{H}_2\text{O})(\text{D}_2\text{O})_{19}$  with one  $\text{H}_2\text{O}$  molecule occupying the ADD site, obtained by probing the frequency labeled by the orange arrow.  $\Delta_{\text{intra}}$  indicates the intramolecular coupling between OH groups. (C) vibrational predissociation spectrum of  $\text{CH}_3\text{NH}_3^+\cdot(\text{H}_2\text{O})_{20}$ , where  $\Delta_{\text{inter}}$  indicates the shift in the OH frequency going from  $\text{H}_2\text{O}$  to HDO which reflects intermolecular coupling. (D) vibrational predissociation spectrum of  $\text{Cs}^+\cdot(\text{H}_2\text{O})_{20}$ . (E) vibrational predissociation spectrum of  $\text{Cs}^+\cdot(\text{H}_2\text{O})_{20}$  (gray trace) and  $\text{Cs}^+\cdot(\text{H}_2\text{O})(\text{D}_2\text{O})_{19}$  (orange trace).

371 the activity from the ADD site was observed in the previous  
 372 study of  $\text{Cs}^+\cdot(\text{H}_2\text{O})_{20}$ .<sup>10</sup> Because the cage in  $\text{Cs}^+\cdot(\text{H}_2\text{O})_{20}$  is  
 373 most symmetrical of the PD series, we extended these  
 374 measurements to the  $\text{CH}_3\text{NH}_3^+$ ,  $\text{Li}^+$ , and  $\text{Na}^+$  systems. The  
 375 results are displayed along with the earlier  $\text{Cs}^+$  spectra in Figure  
 376 5D. Interestingly, all of the activity in the  $3400\text{--}3600\text{ cm}^{-1}$   
 377 range not associated with AD bands appears as a doublet with  
 378 about same splitting and intensity distribution such that the  
 379 higher energy member dominates the lower feature by about a  
 380 factor of 2. The doublet splitting and intensity distribution are  
 381 quite similar in all cases except the  $\text{Na}^+$  spectrum (Figure 5D4),  
 382 which appears broader than those below and above it, an effect  
 383 likely due to overlapping bands. Note that the range of simulated  
 384 ADD behavior at the interface (top trace) encompasses that  
 385 observed experimentally. The fact that these heterogeneous  
 386 contributions to the spectrum in the  $3500\text{ cm}^{-1}$  region occur  
 387 with similar shapes is surprising and significant. The center  
 388 frequency of the doublet motif appears to be simply displaced  
 389 across the predicted region. The issue of whether the ADD  
 390 doublet arises from the coupling between the OH oscillators  
 391 when a water molecule is embedded in a network is important, as  
 392 it involves the question of whether the localized oscillators are  
 393 degenerate in that binding site (for example using HDO). The  
 394 observation that the centroid of the doublet motif evolves over  
 395  $100\text{ cm}^{-1}$ , about the same energy as the splitting between the  
 396 peaks, while maintaining a similar intensity profile suggests that  
 397 this splitting is indeed mostly due to the intramolecular  
 398 coupling, as opposed to “diagonal disorder” in the local force  
 399 constants.<sup>2</sup> We explored this issue in the case of the  $\text{CH}_3\text{NH}_3^+$   
 400 system by comparing the site specific ADD pattern from the  
 401  $\text{CH}_3\text{ND}_3^+\cdot(\text{H}_2\text{O})(\text{D}_2\text{O})_{19}$  cluster with that of the  $\text{CH}_3\text{ND}_3^+\cdot$   
 402  $(\text{HDO})(\text{D}_2\text{O})_{19}$  cluster with the result presented in Figure 6A–  
 403 C. The highest energy feature ( $\text{OH}_{\text{ADD}}^{\text{high}}$ ) in the ADD region  
 404 arising from the single OH oscillator (in HDO) red-shifts by  
 405  $\sim 36\text{ cm}^{-1}$  ( $\Delta_{\text{intra}}$ ) relative the high energy edge of the ADD  
 406 feature (Figure 6B) from  $\text{CH}_3\text{ND}_3^+\cdot(\text{H}_2\text{O})(\text{D}_2\text{O})_{19}$ . The local  
 407 OH oscillator in HDO thus falls roughly midway between the  
 408 ADD doublet (Figure 6B), confirming significant intramolecular

coupling between the two OH oscillators on the same ADD  
 409  $\text{H}_2\text{O}$  molecule.

We note that the high energy edge of the ADD band structure  
 411 in the  $\text{CH}_3\text{NH}_3^+\cdot(\text{H}_2\text{O})_{20}$  (Figure 6C) is slightly ( $\Delta_{\text{inter}} \sim 3\text{ cm}^{-1}$ ) blue-shifted  
 412 relative to the ADD bands in the isolated  
 413  $\text{H}_2\text{O}$  (Figure 6B). This is consistent with a contribution from  
 414 intermolecular coupling between  $\text{H}_2\text{O}$  molecules in the  
 415 homogeneous isotopologue. The direction and magnitude of  
 416 this shift was also observed in the case of  $\text{Cs}^+\cdot(\text{H}_2\text{O})_{20}$ , with an  
 417 expanded view in Figure 6D,E. In this case, the leading edge of  
 418 the ADD band structure blue-shifts when replacing all  $\text{D}_2\text{O}$   
 419 molecules with  $\text{H}_2\text{O}$  molecules by  $\Delta_{\text{inter}} \sim 14\text{ cm}^{-1}$ .

### III. QUALITATIVE INTERPRETATION OF TRENDS AND THEORETICAL ANALYSIS OF THE NETWORK TOPOLOGIES THAT DRIVE THE LOCAL OH FREQUENCIES OF EMBEDDED WATER MOLECULES: CONTRIBUTIONS FROM THE SECOND HYDRATION SHELL AND BEYOND

The general trend in the OH frequencies of the AD and AAD sites is revealed to be  $\nu_{\text{AD}}^{\text{free}} > \nu_{\text{AAD}}^{\text{free}} > \nu_{\text{AD}}^{\text{b}} > \nu_{\text{AAD}}^{\text{b}}$ . Qualitatively, we can rationalize this behavior as reflecting the decrease in the effective force constants of both the OH groups when a water molecule accepts a hydrogen bond. When the water molecule has a  $\text{OH}^{\text{free}}$  group, its  $\text{OH}^{\text{b}}$  frequency is lowered incrementally with the number of H-bonds it accepts. This general trend is also displayed when  $\text{H}_2\text{O}$  binds to metal cations: the presence of positive charge that attracts the electrons on oxygen weakens the bonds to the hydrogen atoms, effectively pushing the positively charged protons away. At the extreme, we note that the OH stretches in  $\text{H}_2\text{O}^+$  are  $\sim 500\text{ cm}^{-1}$  lower than those in  $\text{H}_2\text{O}$ <sup>39,40</sup> reflecting the connection between the effective force constant and the electron density around the OH bond. Characterization of the H-bonding strength in the context of partial charge transfer has been discussed at length in the context of the isomers formed by the neutral water hexamer.<sup>5,41</sup> What accounts for the large frequency ranges exhibited by the AAD and AADD sites, given that they all share the same local coordination

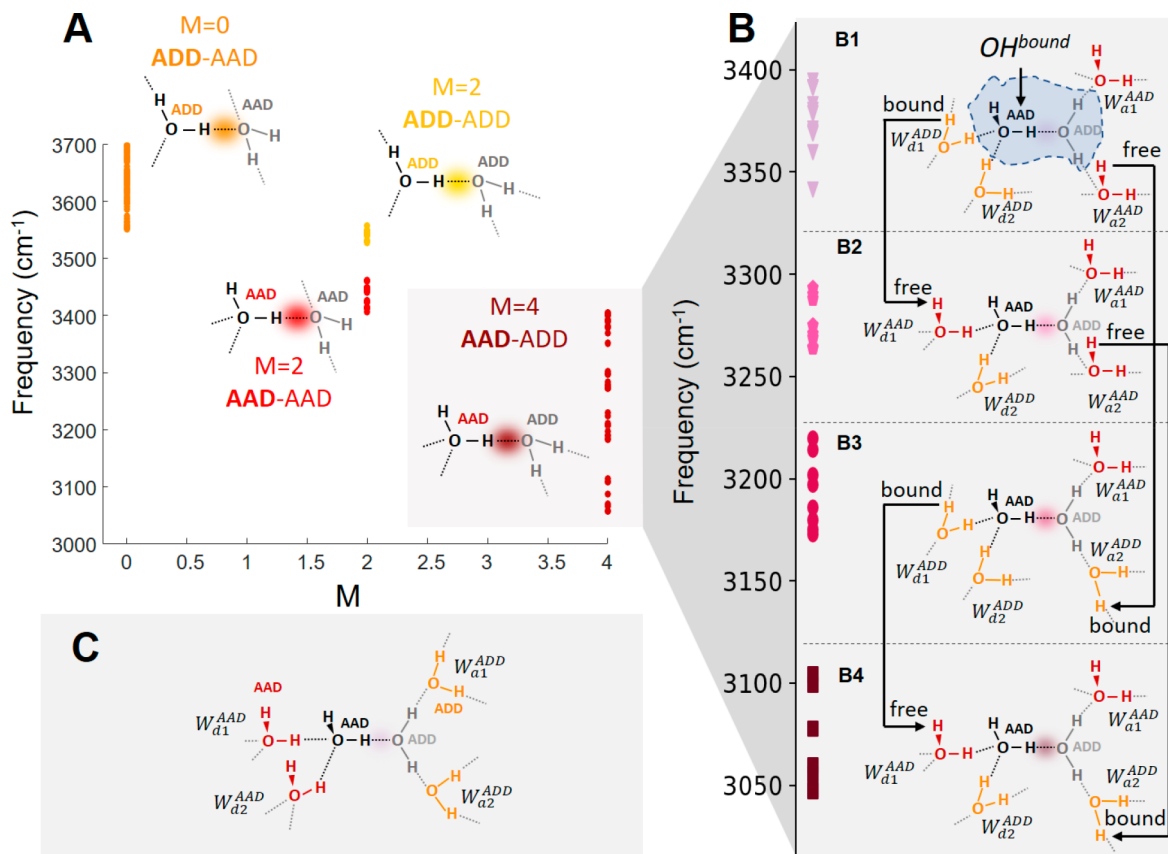


**Figure 7.** Calculated bound OH frequencies in isomers of the  $\text{Cs}^+(\text{H}_2\text{O})(\text{D}_2\text{O})_{19}$  classified by their hydrogen bond environments. (A) Harmonic frequencies of the bound OH groups plotted against the  $M$  index proposed by Ohno.<sup>3</sup> These points are further classified and color coded with an index proposed by Skinner and co-workers, which capture the binding type of both the donor and acceptor water molecules of the H-bond of interest. The schematic structures are shown as water dimers. For example, AAD-ADD corresponds to the case where an OH group on an AAD water molecule donates to an ADD water molecule. The OH oscillators indexed by  $M = 4$  (or AAD-ADD) are again further classified in (B) by the binding types of water molecules surrounding the dimer ( $W_a$  and  $W_d$ ). B1 and C represent the environments that yield the weakest and strongest H-bond in the central dimer, respectively. B1–B4 are the structures present in the clusters. The black arrows label the change of exterior water molecule's type from one class to another.

arrangement? One correlation that accounts for long-range interactions is the dependence of the  $\text{OH}^b$  frequencies on the net local electric field at the bond center.<sup>2,38</sup> Skinner and Ohno<sup>3,5</sup> have developed schemes to classify this dependence according to the local network topology. Those maps were generated by exploiting experimental results on the frequencies of the neutral water hexamer to calibrate the methods, and then use these calculations to follow how they are modified in the various isomeric forms. In the scheme reported by Ohno,<sup>3</sup> the index,  $M$ , is defined as

$$M = -d' + a' + d'' - a'' \quad (1)$$

where  $d'$  (0 or 1) and  $a'$  (0, 1 or 2) denote the number of additional donor ( $d'$ ) and acceptor ( $a'$ ) H-bonds engaged by the molecule with the  $\text{OH}^b$  group (gray dashed bonds on the structures in Figure 7A). Similarly,  $d''$  (0, 1, or 2) and  $a''$  (0 or 1) label the number of additional donor and acceptor H-bonds on the water tethered to  $\text{OH}^b$ . For a specific example, the AAD-ADD pair of water molecules displayed in the lower right of Figure 7A has the value  $M = -0 + 2 + 2 - 0 = 4$ . The points in Figure 7A are the calculated  $\text{OH}^b$  frequencies of all the OH groups in the  $\text{Cs}^+(\text{H}_2\text{O})(\text{D}_2\text{O})_{19}$  PD cage structure, sorted by the  $M$  values that encode their H-bonding environments. Indeed, there is a general trend for lower  $\text{OH}^b$  frequencies with larger  $M$  values, but note that the systems identified by  $M = 4$  are

calculated to vary by  $\sim 350 \text{ cm}^{-1}$ . Thus, it is evident that variations in the more extended surrounding network must be taken into account to recover the local  $\text{OH}^b$  behavior.

A useful ansatz that rationalizes the dependence of  $\text{OH}^b$  frequencies on the surrounding network topology casts a strong H-bond as a frustrated intermolecular proton transfer reaction.<sup>42,43</sup> In that picture, the frequency of the OH group reflects the local endothermicity of this reaction. This is, in turn, determined by how well the extended H-bonding configuration could solvate the incipient  $\text{H}_3\text{O}^+$  and  $\text{OH}^-$  ion pair generated by proton transfer.<sup>9</sup> This situation is illustrated in the set of configurations presented in Figure 7B, which focuses on the AAD site in the specific situation where the donor binds to an ADD molecule, an arrangement that corresponds to  $M = 4$  according to eq 1. The key issue is to explore the role played by the site environments occupied by the four molecules solvating the water dimer bound together by the  $\text{OH}^b$  group (black AAD and gray ADD in dashed box, Figure 7B1). Two of these donate ( $W_d$ ) and two accept ( $W_a$ ) H-bonds at the four contact points indicated in Figure 7B1. Both  $\text{H}_3\text{O}^+$  and  $\text{OH}^-$  ions adopt 3-fold hydration shells at the interface and in clusters.<sup>44–46</sup> In the case of  $\text{H}_3\text{O}^+$ , the three molecules in the first hydration shell reside in ADD sites,<sup>24,44,47</sup> while those in the first shell around hydroxide adopt the AAD configuration.<sup>48</sup> This is the scenario depicted in Figure 7C when applied to the pair of water molecules bound by

494 OH<sup>b</sup>. By similar reasoning, the arrangement displayed in Figure 495 7B1 offers the poorest hydration environment since both  $W_a$  and 496  $W_d$  water molecules now reside in sites opposite to those that 497 best solvate the ion pair. The calculated frequencies of the OH<sup>b</sup> 498 sites with Figure 7B1 structures are indeed the least red-shifted 499 and form a distinct group near 3375 cm<sup>-1</sup>. Unfortunately, the 500 favorable Figure 7C arrangement does not occur in the low 501 energy forms of the Cs<sup>+</sup>·(H<sub>2</sub>O)<sub>20</sub> PD cage structure. A recent 502 theoretical investigation of the (H<sub>2</sub>O)<sub>20</sub> cluster reported that 503 this arrangement indeed yields the strongest hydrogen bond.<sup>49</sup> 504 Nonetheless, it is instructive to incrementally change the site 505 classes of the four outer water molecules ( $W_a$  and  $W_d$  in Figure 506 7B, gray box) into the more favorable sites, starting from the 7B1 507 motif. For example, changing a donor water ( $W_{d1}$ ) from ADD 508 (denoted as  $W_{d1}^{ADD}$ ) to the AAD (denoted as  $W_{d1}^{AAD}$ ) orientation 509 with a free OH group yields the Figure 7B2 hydration topology, 510 which indeed identifies a common hydration motif shared by the 511 OH<sup>b</sup> oscillators with frequencies around 3275 cm<sup>-1</sup> (panel 512 Figure 7B2). On the other hand, changing a  $W_{a2}^{ADD}$  water to the 513  $W_{a2}^{AAD}$  motif yields the network structure indicated in 7B3, which 514 is the environment common to the OH<sup>b</sup> transitions near 3200 515 cm<sup>-1</sup>. Note that this group occurs with about twice the shift 516 (relative to the Figure 7B1 class) as those in the Figure 7B2 517 panel. Interestingly, a similar change in frequency occurs when 518 the one of the  $W_a$  waters in the Figure 7B2 structure is switched 519 from AAD to ADD, thus generating the Figure 7B4 arrangement. 520 That topology is common to the group of OH<sup>b</sup> transitions 521 near 3075 cm<sup>-1</sup>, the most red-shifted of the OH<sup>b</sup> stretches 522 calculated for this PD structure.

523 The trends displayed in Figure 7B thus elucidate the structural 524 variations experienced by an OH<sup>b</sup> group that is most simply 525 described as in an AAD-ADD,  $M = 4$  local environment. The 526 calculated frequency groupings in Figure 7B are distinct because 527 we have focused on the structurally well-defined PD cage in Cs<sup>+</sup>· 528 (H<sub>2</sub>O)<sub>20</sub>. To introduce a modified index that describes this 529 extended topological dependence of the OH<sup>b</sup> shifts, we first note 530 that the  $W_a^{ADD} \rightarrow W_a^{AAD}$  conversion yields about twice the shift as 531 that found for  $W_d^{ADD} \rightarrow W_d^{AAD}$ . One way to classify the 532 frequencies associated with the four arrangements is to count the 533 number of hydrogen bonds in  $W_a$  and  $W_d$  water molecules 534 associated with the solvent structure and account for the fact 535 that changing the bonding to the  $W_a$  water molecules induces 536 about twice the shift as do those involving the  $W_d$  molecules. A 537 scheme that accounts for the OH<sup>b</sup> location for various possible 538  $W_{a,d}$  arrangements with the same  $M$  value is provided by  $M'$ :

$$M' = M + \frac{-d'^{(2)} + a'^{(2)}}{8} + \frac{d''^{(2)} - a''^{(2)}}{4} \quad (2)$$

540 where  $M$  is the index defined in eq 1 and the additional terms 541 capture the shifts induced by the configurations of the  $W_{a,d}$  542 molecules. Specifically,  $a'^{(2)}$  and  $d'^{(2)}$  are the total number of 543 extra acceptor and donor H-bonds in the  $W_d$  water molecules 544 ( $W_{d1}$  and  $W_{d2}$  in Figure 7B) apart from those to the dimer of 545 interest, whereas  $a''^{(2)}$  and  $d''^{(2)}$  are the total number of extra 546 acceptor and donor hydrogen bonds in the  $W_a$  molecules 547 excluding the ones to the dimer ( $W_{a1}$  and  $W_{a2}$  in Figure 7B). The 548 ' and " denote the donor and acceptor sides of the dimer, which 549 follows the convention established in eq 1. The (2) labels 550 emphasize that the H-bonds belong to the second hydration 551 shell. Several example calculations of the  $M'$  are provided in 552 Figure S11. The performance of this index when applied to all of 553 the site configurations in this work is presented in Figure 8. The

554 index thus captures the effect of the sites occupied by water 555 molecules in the first and second hydration shells around a 555 particular OH group. 556

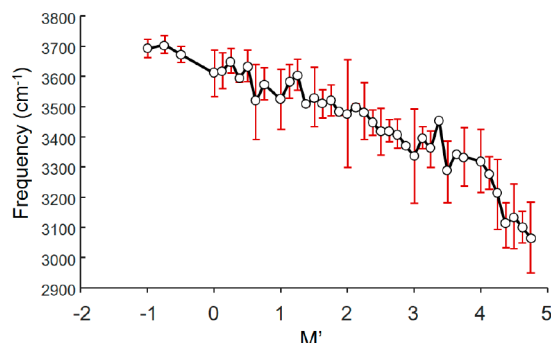


**Figure 8.** Calculated bound OH frequencies in various water cluster ions sorted by their  $M'$  index, defined by eq 2. Harmonic frequency calculations for isomers of the  $M^+ \cdot (H_2O) \cdot (D_2O)_{n-1}$  ( $M = Li, Na, Cs, ND_4, CD_3NH_3$ , and  $n = 20$ ) clusters were done at the B3LYP/6-31+G\*\* level of theory and basis with the LANL2DZ pseudopotential for Cs. Frequencies were scaled by 0.973.

557 Qualitatively, the  $M'$  index reflects the cooperativity and 558 anticooperativity effects caused by the water molecules 559 surrounding the dimer bound by OH<sup>b</sup>. In general, when the 560  $W_d$  water molecules accept one or more H-bonds (larger  $a'^{(2)}$ ), 561 the strength of the OH<sup>b</sup> bond increases, which is again a 562 statement of cooperativity. The degree of cooperativity depends 563 on the strength of the H-bond between the  $W_d$  water molecule 564 and the OH<sup>b</sup>. This is most effective when a  $W_d$  molecule accepts 565 two H-bonds and retains the free OH, making its contributions 566 to  $d'^{(2)}$  and  $a'^{(2)}$  zero and two, respectively. On the other hand, a 567  $W_a$  water molecule strengthens the H-bond to OH<sup>b</sup> the most 568 when it donates two H-bonds (making its contribution to  $d''^{(2)} = 2$ ) 569 and accepts no additional hydrogen bonds (making its 570 contribution to  $a''^{(2)} = 0$ ). An interesting observation is that  $W_a$  571 molecules have roughly twice the impact on the H-bond 572 strength than do  $W_d$  molecules (an effect accommodated by the 573 1/4 vs 1/8 factors in eq 2). 573

574 The above discussion focused on an empirical connection 575 between the shape of the surrounding network and the OH<sup>b</sup> 576 frequency using arguments based on shifts in the electron 577 density. To address the underlying changes in bonding that drive 578 these values, we turn to electronic structure calculations to 579 explore the changes in the electron density in the region of the 580 oxygen atom of the accepting water molecule for various 581 hydrogen bonding geometries depicted in Figure 7B. Specifically, 582 when a hydrogen bond is formed, we expect an increase in 583 electron density ( $\delta_{HB}$ ) between the hydrogen atom in the 584 donating water molecule and the oxygen atom in the accepting 585 water molecule along with a decrease in electron density ( $\delta_{OH}$ ) 586 in the region of the OH bond in the donating water molecule. 587 We explored changes to the electron density in these two regions 588 as the strength of the hydrogen bond is tuned through the 589 environments of the donor and acceptor water molecules. We 590 applied this procedure to follow changes in the electronic 591 structure when a water dimer is embedded in a solvation shell of 592 zero to six water molecules (up to three on the open 593 coordination sites on each water). Details are included in the 594 supporting materials (section SIV). On the basis of the results 595 for the analysis of these model systems, we characterize changes 596 in the electron density ( $\delta_e$ ) in terms of the differences in the 596

597 integrated electron density in the hydrogen bond region ( $\delta_{\text{HB}}$ )  
 598 and along the OH bond that donates into the hydrogen bond  
 599 ( $\delta_{\text{OH}}$ ) when additional water molecules are allowed to form a  
 600 hydrogen bonding network with the hydrogen bonding pair of  
 601 water molecules of interest. This analysis is applied to each of the  
 602 hydrogen bonds in the  $\text{Cs}^+(\text{H}_2\text{O})_{20}$  pentagonal dodecahedron  
 603 structure where the other 18 water molecules provide the  
 604 additional hydrogen bonding network. Specifically, electron  
 605 density changes are calculated by taking difference between the  
 606 electron density in the hydrogen bonding region when the pair  
 607 of water molecules is incorporated in the  $(\text{H}_2\text{O})_{20}$  cage relative  
 608 to the electron density of the isolated dimer. The structures of  
 609 the donor/acceptor pair of water molecules are the same for  
 610 both calculations. The effect of the environment on the strength  
 611 of the hydrogen bond of interest is thus captured by  $\delta_e = \delta_{\text{HB}} -$   
 612  $\delta_{\text{OH}}$ . Structures where the solvation environment leads to a  
 613 stronger hydrogen bond (and hence lower frequency) will have  
 614  $\delta_{\text{HB}} > 0$  and  $\delta_{\text{OH}} < 0$ , making  $\delta_e$  positive.

615 In Figure 9, we plot the harmonic OH<sup>b</sup> frequencies of all  
 616 hydrogen-bonded OH stretches in five low energy isomers of

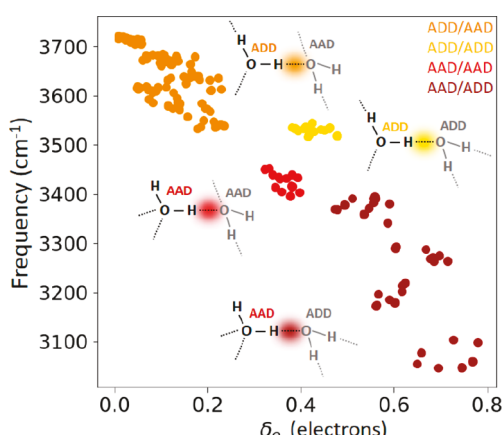


Figure 9. Bound OH frequency dependence on changes in the electron density in the donor OH group and the region along the hydrogen bond. Calculations are carried for the pentagonal dodecahedron cage structure of  $\text{Cs}^+(\text{H}_2\text{O})(\text{D}_2\text{O})_{19}$ . Changes are relative to the densities in the isolated water dimer, held fixed at the geometry of each motif in the cage.

617  $\text{Cs}^+(\text{H}_2\text{O})(\text{D}_2\text{O})_{19}$  as a function of  $\delta_e$ . The colors are used to  
 618 differentiate the types of water molecules involved in these  
 619 hydrogen bonds. As expected from the above discussion, the red  
 620 shift of the hydrogen-bonded OH bond increases with electron  
 621 density in the hydrogen-bonding region. We can further explore  
 622 these effects by identifying the second solvation shell environ-  
 623 ment for the hydrogen bonds formed between AAD and ADD  
 624 water molecules (shown in red). The OH bonds with the lowest  
 625 frequency (and highest electron density in the hydrogen-  
 626 bonding region) are those for which the acceptor water molecule  
 627 is donating to an ADD and an AAD water molecule. The higher  
 628 frequency OH<sup>b</sup> groups donate to two AAD water molecules. As  
 629 discussed above, and seen in Figure 9, hydrogen bonds to ADD  
 630 water molecules are stronger (lower frequency) than ones to  
 631 AAD water molecules when the donor molecule is in the same  
 632 environment.

#### IV. SUMMARY

633 We have isolated the intrinsic spectral signatures of the OH  
 634 stretching motions on a single water molecule embedded at

various sites within the water cage structures that assemble 635 around atomic and molecular cations. This is accomplished 636 using an isotopic labeling scheme in which a single intact  $\text{H}_2\text{O}$  637 molecule is incorporated into an otherwise perdeuterated cage. 638 The site-specific spectra are then extracted by carrying out two- 639 color, IR-IR photobleaching in an isotopomer-selective mode. 640 The specific patterns recovered with this approach are quite 641 simple, generally consisting of one to three localized absorptions 642 arising from the two correlated fundamentals on the OH groups 643 of the same water molecule. The only complication to this 644 pattern is the appearance of a third band when the red-shifted 645 OH bands fall near the overtone of the HOH intramolecular 646 bending vibration at  $\sim 3200 \text{ cm}^{-1}$ . Different characteristic 647 patterns are observed for the five binding sites in play at the 648 air-water interface, which differ according to the number of 649 donor and acceptor H-bonds: A, AD, AAD, ADD, and AADD. 650 Although the patterns are preserved in many systems, the 651 frequency ranges over which they appear depend strongly on the 652 site type, with the largest excursions displayed by the sites that 653 yield larger red-shifts (i.e., AAD > AADD > ADD > AD > A). The 654 simple doublet structure of isolated water arising from the 655 symmetric and antisymmetric OH stretch normal modes is 656 preserved in the ADD sites but with a splitting reduced by about 657 20%. The AADD sites are the most difficult to characterize 658 because they are embedded in overlapping band structures. 659 Deconvolution yields a single, broadened feature, suggesting 660 suppression of the coupling between the OH groups. These 661 results provide a diverse learning set with which to construct 662 extended frequency maps that describe how the IR fundamental 663 of an embedded OH oscillator depends on the topology of the 664 extended water network and does so in systems that can be 665 treated with accurate theoretical methods.<sup>50-53</sup> 666

#### ASSOCIATED CONTENT

##### Supporting Information

The Supporting Information is available free of charge at 669  
<https://pubs.acs.org/doi/10.1021/acs.jpca.0c07795>. 670

Supporting experimental and computational data, SFG 671  
 intensity spectra, vibrational spectra,  $\text{MS}^3\text{IR}^2$  instrument, 672  
 dependence of OH oscillator's frequency on the H-bond 673  
 environments, calculations of the  $M'$  index, rotatable 674  
 structures, electron density maps,  $\delta_e$  vs  $M$ , and tables of 675  
 number of water molecules in the cluster, Z-matrix values, 676  
 optimized parameters, and Cartesian coordinates (PDF) 677  
 Coordinates of the optimized structures and harmonic 678  
 frequency for  $\text{M}^+(\text{H}_2\text{O})(\text{D}_2\text{O})_{19}$  (ZIP) 679

#### AUTHOR INFORMATION

##### Corresponding Author

Mark A. Johnson – *Sterling Chemistry Laboratory, Yale* 682  
*University, New Haven, Connecticut 06520, United States;* 683  
 • [orcid.org/0000-0002-1492-6993](https://orcid.org/0000-0002-1492-6993); 684  
 Email: [mark.johnson@yale.edu](mailto:mark.johnson@yale.edu) 685

##### Authors

Nan Yang – *Sterling Chemistry Laboratory, Yale University,* 687  
*New Haven, Connecticut 06520, United States;* • [orcid.org/0000-0003-1253-2154](https://orcid.org/0000-0003-1253-2154) 688  
 689  
 Thien Khuu – *Sterling Chemistry Laboratory, Yale University,* 690  
*New Haven, Connecticut 06520, United States;* • [orcid.org/0000-0003-0386-2450](https://orcid.org/0000-0003-0386-2450) 691  
 692

693 **Sayoni Mitra** – *Sterling Chemistry Laboratory, Yale University,*  
694 *New Haven, Connecticut 06520, United States*  
695 **Chinh H. Duong** – *Sterling Chemistry Laboratory, Yale*  
696 *University, New Haven, Connecticut 06520, United States;*  
697 [DOI orcid.org/0000-0001-8026-1371](https://orcid.org/0000-0001-8026-1371)  
698 **Ryan J. DiRisio** – *Department of Chemistry, University of*  
699 *Washington, Seattle, Washington 98195, United States;*  
700 [DOI orcid.org/0000-0003-1272-0112](https://orcid.org/0000-0003-1272-0112)  
701 **Anne B. McCoy** – *Department of Chemistry, University of*  
702 *Washington, Seattle, Washington 98195, United States;*  
703 [DOI orcid.org/0000-0001-6851-6634](https://orcid.org/0000-0001-6851-6634)  
704 **Evangelos Miliordos** – *Advanced Computing, Mathematics*  
705 *and Data Division, Pacific Northwest National Laboratory,*  
706 *Richland, Washington 99352, United States;* [DOI orcid.org/0000-0003-3471-7133](https://orcid.org/0000-0003-3471-7133)  
707 **Sotiris S. Xantheas** – *Department of Chemistry, University of*  
708 *Washington, Seattle, Washington 98195, United States;*  
709 *Advanced Computing, Mathematics and Data Division, Pacific*  
710 *Northwest National Laboratory, Richland, Washington*  
711 *99352, United States;* [DOI orcid.org/0000-0002-6303-1037](https://orcid.org/0000-0002-6303-1037)

713 Complete contact information is available at:

714 <https://pubs.acs.org/10.1021/acs.jpca.0c07795>

## 715 Notes

716 The authors declare no competing financial interest.

## 717 Biographies



718 Nan Yang received his B.S. degree in Chemistry from University of  
719 Rochester (2015). His undergraduate research was on ion optics design  
720 and simulations to optimize velocity map imaging instruments for ion-  
721 radical cross beam reactions with James M. Farrar. He is currently a  
722 Ph.D. student at Yale University working for Mark A. Johnson. His  
723 research interests include instrument development for cryogenic ion  
724 vibrational photodissociation spectroscopy, the mechanistic study of  
725 water's vibrational spectra using ionic water clusters, and the  
726 temperature and time dependent study of water reorientation in a  
727 hydrogen bond network and the resulting spectral diffusion.



728 Thien Khuu received his B.S. in Chemistry from Tufts University as a  
729 Questbridge Scholar in 2018 where he performed undergraduate  
730 research with M. J. Shultz. He is currently a third-year graduate student  
731 in Mark Johnson's lab at Yale University pursuing his Ph.D. in Physical  
732 Chemistry. His primary research interests are in studying proton  
733 transfer mechanisms in various chemical and biological systems using  
734 ion spectroscopy.



735 Sayoni Mitra is currently a fourth year Ph.D. candidate in the Johnson  
736 Lab at Yale University. Her research interests include understanding the  
737 structure and mechanism of acid dissociation in ionic water clusters and  
738 its temperature dependence, using cryogenic IR spectroscopy. She  
739 received her Integrated B.S.-M.S. degree from National Institute of  
740 Science Education and Research, India, in 2017, where she performed  
741 computational studies on the mechanisms and dynamics of  
742 halogenophilic reactions.



743 Chinh H. Duong received his B.A. degree with high honors in  
744 Chemistry from Wesleyan University (2013) and Ph.D. degree in  
745 Chemistry from Yale University (2019). His undergraduate research,  
746 under the mentorship of Stewart E. Novick, was on the structural  
747

747 characterization of perfluoroalkanes and van der Waals complexes with  
748 microwave spectroscopy. He is an NSF GRP Fellow and Gates  
749 Millennium Scholar. His graduate research in the Mark A. Johnson  
750 group included designing instrumentation for handling, reacting, and  
751 characterizing sensitive cryogenic ions and their reaction intermediates,  
752 in addition to studying excess proton behaviors within flexible and rigid  
753 frameworks.



754 Mark Johnson received his B.S. degree in chemistry from the University  
755 of California at Berkeley (1977) where he carried out undergraduate  
756 research with C. Bradley Moore. He then obtained his Ph.D. in  
757 chemistry at Stanford University (1983) with Richard Zare, followed by  
758 a postdoc with W. Carl Lineberger (1983–85) at JILA and the  
759 University of Colorado at Boulder. He joined the chemistry faculty at  
760 Yale University in 1985 where he is currently the Arthur T. Kemp  
761 Professor of Chemistry. His main research interests are in the  
762 development and exploitation of ion chemistry and spectroscopy as a  
763 means through which to understand the physical origins of macroscopic  
764 behavior at the molecular level. He is currently the co-editor of the  
765 *Annual Review of Physical Chemistry*.



766 Ryan J. DiRisio is a fourth year Ph.D. candidate in Anne McCoy's group  
767 at the University of Washington. His research focuses on understanding  
768 the role of nuclear quantum effects in aqueous hydrogen bonding and  
769 proton transfer. He studies the structure of protonated water clusters  
770 and the vibrational couplings in them, which can then be related to  
771 vibrational spectroscopy. These investigations are done predominantly  
772 through the use of diffusion Monte Carlo. Ryan earned his B.S. in  
773 Chemistry from the College of William and Mary in 2017.



774 Anne McCoy received her B.S. degree in chemistry from Haverford  
775 College (1987) and her Ph.D. from the University of Wisconsin—  
776 Madison (1992) with E. L. Sibert. After working as a postdoctoral  
777 associate with R. B. Gerber at Hebrew University and the University of  
778 California, Irvine (1992–1994), she joined the faculty at The Ohio  
779 State University. In 2015, she moved to the University of Washington,  
780 where she is the Natt-Lingafelter Endowed Professor. She is currently  
781 the Deputy Editor for *J. Phys. Chem. A* and the immediate past chair of  
782 the PHYS division of the ACS.



783 Evangelos Miliordos is currently the James E. Land Assistant Professor  
784 of Chemistry at Auburn University. His research focuses on high level  
785 electronic structure calculations on transition metal compounds and  
786 catalyzed reactions for the functionalization of methane and utilization  
787 of CO<sub>2</sub>. He earned his Ph.D. in Computational Chemistry from the  
788 National and Kapodistrian University of Athens, Greece, in 2010. He  
789 moved to the United States to pursue his postdoctoral work at Michigan  
790 State University with Professor Katharine Hunt on weak molecular  
791 interactions. In 2012, he moved to the Pacific Northwest National  
792 Laboratory as a post-doctoral fellow under the supervision of Dr. Sotiris  
793 Xantheas, where he worked primarily on microsolvated systems. In  
794 2015, he moved to the University of Delaware to work on catalysis with  
795 Professor Dionisis Vlachos, and in 2016 he accepted his current  
796 position at Auburn University. He has published more than thirty  
797 articles as an independent researcher and he recently received the NSF  
798 CAREER award.



799 Sotiris Xantheas is a Laboratory Fellow in the Advanced Computing,  
 800 Mathematics and Data Division at Pacific Northwest National  
 801 Laboratory in Richland, WA, a UW-PNNL Distinguished Faculty  
 802 Fellow in the Department of Chemistry at the University of Washington  
 803 in Seattle, WA, and a Specially Appointed Professor in the World  
 804 Research Hub Initiative at the Tokyo Institute of Technology in Tokyo,  
 805 Japan. He has received several honors and awards, including a recent  
 806 appointment as Gauss Professor at the University of Göttingen,  
 807 Germany, the "Friedrich Wilhelm Bessel" Award from the Alexander  
 808 von Humboldt Foundation, the Director's Award for Outstanding  
 809 Performance at PNNL (twice), and a Fulbright Scholarship from the  
 810 Institute of International Education. He is a Fellow of the American  
 811 Physical Society (APS), the American Association for the Advancement  
 812 of Science (AAAS), a visiting Fellow at the Institute for Advanced Study  
 813 (IAS) of the Technical University of Munich at Garching, Germany, a  
 814 Fellow of the Japan Society for the Promotion of Science (JSPS) and a  
 815 Marie Curie Fellow at the Institute of Electronic Structure & Laser in  
 816 Heraklion, Greece. He has published over 180 papers and chapters in  
 817 books and he has presented over 250 invited lectures at scientific  
 818 institutions and professional meetings.

## 819 ■ ACKNOWLEDGMENTS

820 M.A.J. thanks the Chemistry Division of the National Science  
 821 Foundation for supporting this work under grant CHE-  
 822 1900119. The IR-IR photofragmentation mass spectrometer  
 823 crucial for this work was developed under AFOSR DURIP grant  
 824 FA9550-17-1-0267. A.B.M. thanks the Chemistry division of the  
 825 National Science Foundation for supporting this work under  
 826 grant CHE-1856125. Parts of this work were performed using  
 827 the Ilahie cluster, which was purchased using funds from an MRI  
 828 grant from the National Science Foundation (CHE-1624430).  
 829 E.M. and S.S.X. acknowledge support from the US Department  
 830 of Energy, Office of Science, Office of Basic Energy Sciences,  
 831 Division of Chemical Sciences, Geosciences and Biosciences at  
 832 Pacific Northwest National Laboratory (PNNL). PNNL is a  
 833 multiprogram national laboratory operated for DOE by Battelle.  
 834 This research also used resources of the National Energy  
 835 Research Scientific Computing Center, which is supported by  
 836 the Office of Science of the U.S. Department of Energy under  
 837 Contract No. DE-AC02-05CH11231.

## 838 ■ REFERENCES

- (1) Tainter, C. J.; Ni, Y.; Shi, L.; Skinner, J. L. Hydrogen bonding and OH-stretch spectroscopy in water: hexamer (cage), liquid surface, liquid, and ice. *J. Phys. Chem. Lett.* **2013**, *4* (1), 12–17.
- (2) Gruenbaum, S. M.; Tainter, C. J.; Shi, L.; Ni, Y.; Skinner, J. L. Robustness of Frequency, Transition Dipole, and Coupling Maps for Water Vibrational Spectroscopy. *J. Chem. Theory Comput.* **2013**, *9* (7), 3109–3117.

- (3) Ohno, K.; Okimura, M.; Akai, N.; Katsumoto, Y. The effect of cooperative hydrogen bonding on the OH stretching-band shift for water clusters studied by matrix-isolation infrared spectroscopy and density functional theory. *Phys. Chem. Chem. Phys.* **2005**, *7* (16), 3005–3014.
- (4) Ni, Y. C.; Skinner, J. L. IR and SFG vibrational spectroscopy of the water bend in the bulk liquid and at the liquid-vapor interface, respectively. *J. Chem. Phys.* **2015**, *143* (1), 014502.
- (5) Tainter, C. J.; Skinner, J. L. The water hexamer: three-body interactions, structures, energetics, and OH-stretch spectroscopy at finite temperature. *J. Chem. Phys.* **2012**, *137* (10), 104304.
- (6) Hsieh, C. S.; Okuno, M.; Hunger, J.; Backus, E. H. G.; Nagata, Y.; Bonn, M. Aqueous Heterogeneity at the Air/Water Interface Revealed by 2D-HD-SFG Spectroscopy. *Angew. Chem., Int. Ed.* **2014**, *53* (31), 8146–8149.
- (7) Inoue, K.; Ishiyama, T.; Nihonyanagi, S.; Yamaguchi, S.; Morita, A.; Tahara, T. Efficient Spectral Diffusion at the Air/Water Interface Revealed by Femtosecond Time-Resolved Heterodyne-Detected Vibrational Sum Frequency Generation Spectroscopy. *J. Phys. Chem. Lett.* **2016**, *7* (10), 1811–1815.
- (8) Yang, N.; Duong, C. H.; Kelleher, P. J.; Johnson, M. A.; McCoy, A. B. Isolation of Site-Specific Anharmonicities of Individual Water Molecules in the  $\text{I}^-(\text{H}_2\text{O})_2$  Complex Using Tag-Free, Isotopomer Selective IR-IR Double Resonance. *Chem. Phys. Lett.* **2017**, *690*, 159–171.
- (9) Wolk, A. B.; Leavitt, C. M.; Garand, E.; Johnson, M. A. Cryogenic Ion Chemistry and Spectroscopy. *Acc. Chem. Res.* **2014**, *47* (1), 202–210.
- (10) Yang, N.; Duong, C. H.; Kelleher, P. J.; McCoy, A. B.; Johnson, M. A. Deconstructing Water's Diffuse OH Stretching Vibrational Spectrum With Cold Clusters. *Science* **2019**, *364* (6437), 275–278.
- (11) Zatula, A. S.; Ryding, M. J.; Andersson, P. U.; Uggerud, E. Proton Mobility and Stability of Water Clusters Containing Alkali Metal Ions. *Int. J. Mass Spectrom.* **2012**, *330*, 191–199.
- (12) Ryding, M. J.; Zatula, A. S.; Andersson, P. U.; Uggerud, E. Isotope exchange in reactions between D<sub>2</sub>O and size-selected ionic water clusters containing pyridine, H+(pyridine)(m)(H<sub>2</sub>O)(n). *Phys. Chem. Chem. Phys.* **2011**, *13* (4), 1356–1367.
- (13) Wolke, C. T.; Fournier, J. A.; Miliordos, E.; Kathmann, S. M.; Xantheas, S. S.; Johnson, M. A. Isotopomer-Selective Spectra of a Single Intact H<sub>2</sub>O Molecule in the Cs<sup>+</sup>(D<sub>2</sub>O)<sub>5</sub>H<sub>2</sub>O Isotopologue: Going Beyond Pattern Recognition to Harvest the Structural Information Encoded in Vibrational Spectra. *J. Chem. Phys.* **2016**, *144* (7), No. 074305.
- (14) Schaefer, J.; Backus, E. H. G.; Nagata, Y.; Bonn, M. Both Inter- and Intramolecular Coupling of O-H Groups Determine the Vibrational Response of the Water/Air Interface. *J. Phys. Chem. Lett.* **2016**, *7* (22), 4591–4595.
- (15) Seki, T.; Sun, S. M.; Zhong, K.; Yu, C. C.; Machel, K.; Dreier, L. B.; Backus, E. H. G.; Bonn, M.; Nagata, Y. Unveiling Heterogeneity of Interfacial Water through the Water Bending Mode. *J. Phys. Chem. Lett.* **2019**, *10* (21), 6936–6941.
- (16) Nihonyanagi, S.; Kusaka, R.; Inoue, K.; Adhikari, A.; Yamaguchi, S.; Tahara, T. Accurate determination of complex c(2) spectrum of the air/water interface. *J. Chem. Phys.* **2015**, *143* (12), 124707.
- (17) Kirov, M. V.; Fanourgakis, G. S.; Xantheas, S. S. Identifying the most stable networks in polyhedral water clusters. *Chem. Phys. Lett.* **2008**, *461* (4), 180–188.
- (18) Cooper, R. J.; Chang, T. M.; Williams, E. R. Hydrated Alkali Metal Ions: Spectroscopic Evidence for Clathrates. *J. Phys. Chem. A* **2013**, *117* (30), 6571–6579.
- (19) Gonzalez, B. S.; Hernandez-Rojas, J.; Wales, D. J. Global minima and energetics of Li<sup>+</sup>(H<sub>2</sub>O)<sub>n</sub> and Ca<sup>2+</sup>(H<sub>2</sub>O)<sub>n</sub> clusters for  $n \leq 20$ . *Chem. Phys. Lett.* **2005**, *412* (1–3), 23–28.
- (20) Willow, S. Y.; Singh, N. J.; Kim, K. S. NH4+ Resides Inside the Water 20-mer Cage As Opposed to H3O+, Which Resides on the Surface: A First Principles Molecular Dynamics Simulation Study. *J. Chem. Theory Comput.* **2011**, *7* (11), 3461–3465.

914 (21) Shin, J.-W.; Hammer, N. I.; Diken, E. G.; Johnson, M. A.;  
915 Walters, R. S.; Jaeger, T. D.; Duncan, M. A.; Christie, R. A.; Jordan, K.  
916 D. Infrared signature of structures associated with the  $\text{H}^+(\text{H}_2\text{O})_n$  ( $n = 6$   
917 to 27) clusters. *Science* **2004**, *304* (5674), 1137–1140.  
918 (22) Skinner, J. L.; Pieniazek, P. A.; Gruenbaum, S. M. Vibrational  
919 Spectroscopy of Water at Interfaces. *Acc. Chem. Res.* **2012**, *45* (1), 93–  
920 100.  
921 (23) Fournier, J. A.; Wolke, C. T.; Johnson, C. J.; Johnson, M. A.;  
922 Heine, N.; Gewinner, S.; Schollkopf, W.; Esser, T. K.; Fagiani, M. R.;  
923 Knorke, H.; Asmis, K. R. Site-specific vibrational spectral signatures of  
924 water molecules in the magic  $\text{H}_3\text{O}^+(\text{H}_2\text{O})_{20}$  and  $\text{Cs}^+(\text{H}_2\text{O})_{20}$  clusters.  
925 *Proc. Natl. Acad. Sci. U. S. A.* **2014**, *111* (51), 18132–18137.  
926 (24) Fournier, J. A.; Johnson, C. J.; Wolke, C. T.; Weddle, G. H.;  
927 Wolk, A. B.; Johnson, M. A. Vibrational spectral signature of the proton  
928 defect in the three-dimensional  $\text{H}^+(\text{H}_2\text{O})_{21}$  cluster. *Science* **2014**, *344*  
929 (6187), 1009–1012.  
930 (25) Stachl, C. N.; Williams, E. R. Effects of Temperature on  
931  $\text{Cs}^+(\text{H}_2\text{O})_{20}$  Clathrate Structure. *J. Phys. Chem. Lett.* **2020**, *11*, 6127–  
932 6132.  
933 (26) Xantheas, S. S. Low-lying energy isomers and global minima of  
934 aqueous nanoclusters: Structures and spectroscopic features of the  
935 pentagonal dodecahedron  $(\text{H}_2\text{O})_{20}$  and  $\text{H}_3\text{O}^+(\text{H}_2\text{O})_{20}$ . *Can. J. Chem. Eng.* **2012**, *90* (4), 843–851.  
936 (27) Ceriotti, M.; Fang, W.; Kusalik, P. G.; McKenzie, R. H.;  
937 Michaelides, A.; Morales, M. A.; Markland, T. E. Nuclear Quantum  
938 Effects in Water and Aqueous Systems: Experiment, Theory, and  
939 Current Challenges. *Chem. Rev.* **2016**, *116* (13), 7529–50.  
940 (28) Ceriotti, M.; Cuny, J.; Parrinello, M.; Manolopoulos, D. E.  
941 Nuclear quantum effects and hydrogen bond fluctuations in water. *Proc. Natl. Acad. Sci. U. S. A.* **2013**, *110* (39), 15591–6.  
942 (29) Robertson, W. H.; Weddle, G. H.; Kelley, J. A.; Johnson, M. A.  
943 Solvation of the  $\text{Cl}^-\text{H}_2\text{O}$  Complex in  $\text{CCl}_4$  Clusters: The Effect of  
944 Solvent-Mediated Charge Redistribution on the Ionic H-Bond. *J. Phys. Chem. A* **2002**, *106*, 1205–1209.  
945 (30) McCoy, A. B. The role of electrical anharmonicity in the  
946 association band in the water spectrum. *J. Phys. Chem. B* **2014**, *118* (28),  
947 8286–8294.  
948 (31) McCoy, A. B.; Guasco, T. L.; Leavitt, C. M.; Olesen, S. G.;  
949 Johnson, M. A. Vibrational manifestations of strong non-Condon  
950 effects in the  $\text{H}_3\text{O}^+\text{X}_3$  ( $\text{X} = \text{Ar}, \text{N}_2, \text{CH}_4, \text{H}_2\text{O}$ ) complexes: a possible  
951 explanation for the intensity in the "association band" in the vibrational  
952 spectrum of water. *Phys. Chem. Chem. Phys.* **2012**, *14* (20), 7205–7214.  
953 (32) Roscioli, J. R.; Diken, E. G.; Johnson, M. A.; Horvath, S.; McCoy,  
954 A. B. Prying apart a water molecule with anionic H-bonding: a  
955 comparative spectroscopic study of the  $\text{X}^-\text{H}_2\text{O}$  ( $\text{X} = \text{OH}, \text{O}, \text{F}, \text{Cl}$ , and  
956  $\text{Br}$ ) binary complexes in the 600–3800  $\text{cm}^{-1}$  region. *J. Phys. Chem. A* **2006**, *110* (15), 4943–4952.  
957 (33) Yang, N.; Duong, C. H.; Kelleher, P. J.; Johnson, M. A. Capturing  
958 intrinsic site-dependent spectral signatures and lifetimes of isolated OH  
959 oscillators in extended water networks. *Nat. Chem.* **2020**, *12*, 159–164.  
960 (34) Li, F.; Skinner, J. L. Infrared and Raman line shapes for ice II. II.  
961  $\text{H}_2\text{O}$  and  $\text{D}_2\text{O}$ . *J. Chem. Phys.* **2010**, *133* (24), 244504.  
962 (35) Shimanouchi, T. *Tables of Molecular Vibrational Frequencies*  
963 *Consolidated Volume I*; National Bureau of Standards, 1972; pp 1–160.  
964 (36) Hermansson, K. Electric-field effects on the OH vibrational  
965 frequency and infrared absorption intensity for water. *J. Chem. Phys.* **1993**, *99*, 861–868.  
966 (37) Carnegie, P. D.; Bandyopadhyay, B.; Duncan, M. A. Infrared  
967 Spectroscopy of  $\text{Mn}^+(\text{H}_2\text{O})$  and  $\text{Mn}^{2+}(\text{H}_2\text{O})$  via Argon Complex  
968 Predissociation. *J. Phys. Chem. A* **2011**, *115* (26), 7602–7609.  
969 (38) Kebede, G. G.; Mitev, P. D.; Briels, W. J.; Hermansson, K. Red-  
970 shifting and blue-shifting OH groups on metal oxide surfaces - towards a  
971 unified picture. *Phys. Chem. Chem. Phys.* **2018**, *20* (18), 12678–12687.  
972 (39) Roth, D.; Dopfer, O.; Maier, J. P. Intermolecular potential energy  
973 surface of the proton-bound  $\text{H}_2\text{O}^+\text{He}$  dimer: Ab initio calculations  
974 and IR spectra of the O-H stretch vibrations. *Phys. Chem. Chem. Phys.* **2001**, *3* (12), 2400–2410.  
975 (40) Huet, T. R.; Pursell, C. J.; Ho, W. C.; Dinelli, B. M.; Oka, T. Infrared-Spectroscopy and Equilibrium Structure of  $\text{H}_2\text{O}^+(\text{X})$  over-  
976 Tilde2b1). *J. Chem. Phys.* **1992**, *97* (9), 5977–5987.  
977 (41) Guevara-Vela, J. M.; Romero-Montalvo, E.; Gomez, V. A. M.; Chavez-Calvillo, R.; Garcia-Revilla, M.; Francisco, E.; Pendas, A. M.; Rocha-Rinza, T. Hydrogen Bond Cooperativity and Anticooperativity Within the Water Hexamer. *Phys. Chem. Chem. Phys.* **2016**, *18* (29), 987 19557–19566.  
978 (42) Craig, S. M.; Menges, F. S.; Duong, C. H.; Denton, J. K.; Madison, L. R.; McCoy, A. B.; Johnson, M. A. Hidden Role of Intermolecular Proton Transfer in the Anomalously Diffuse Vibrational Spectrum of a Trapped Hydronium Ion. *Proc. Natl. Acad. Sci. U. S. A.* **2017**, *114* (24), E4706–E4713.  
979 (43) Duong, C. H.; Yang, N.; Johnson, M. A.; DiRisio, R. J.; McCoy, A. B.; Yu, Q.; Bowman, J. M. Disentangling the Complex Vibrational Mechanics of the Protonated Water Trimer by Rational Control of Its Hydrogen Bonds. *J. Phys. Chem. A* **2019**, *123* (37), 7965–7972.  
980 (44) Fournier, J. A.; Wolke, C. T.; Johnson, M. A.; Odbadrakh, T. T.; Jordan, K. D.; Kathmann, S. M.; Xantheas, S. S. Snapshots of proton accommodation at a microscopic water surface: understanding the vibrational spectral signatures of the charge defect in cryogenically cooled  $\text{H}^+(\text{H}_2\text{O})_{n=2-28}$  clusters. *J. Phys. Chem. A* **2015**, *119* (36), 9425–9440.  
981 (45) Robertson, W. H.; Diken, E. G.; Price, E. A.; Shin, J. W.; Johnson, M. A. Spectroscopic determination of the OH- solvation shell in the OH-center dot( $\text{H}_2\text{O}$ )(n) clusters. *Science* **2003**, *299* (5611), 1367–1372.  
982 (46) Mundy, C. J.; Kuo, I. F. W.; Tuckerman, M. E.; Lee, H. S.; Tobias, D. J. Hydroxide Anion at the Air-water Interface. *Chem. Phys. Lett.* **2009**, *481* (1–3), 2–8.  
983 (47) Fournier, J. A.; Wolke, C. T.; Johnson, C. J.; Johnson, M. A.; Heine, N.; Gewinner, S.; Schollkopf, W.; Esser, T. K.; Fagiani, M. R.; Knorke, H.; Asmis, K. R. Site-Specific Vibrational Spectral Signatures of Water Molecules in the Magic  $\text{H}_3\text{O}^+(\text{H}_2\text{O})_{20}$  and  $\text{Cs}^+(\text{H}_2\text{O})_{20}$  Clusters. *Proc. Natl. Acad. Sci. U. S. A.* **2014**, *111* (51), 18132–18137.  
984 (48) Bankura, A.; Chandra, A. Hydration structure and dynamics of a hydroxide ion in water clusters of varying size and temperature: Quantum chemical and ab initio molecular dynamics studies. *Chem. Phys. Lett.* **2012**, *400*, 154–164.  
985 (49) Kananenka, A. A.; Skinner, J. L. Unusually strong hydrogen bond cooperativity in particular  $(\text{H}_2\text{O})_{20}$  clusters. *Phys. Chem. Chem. Phys.* **2020**, *22*, 18124.  
986 (50) Paesani, F.; Voth, G. A. The Properties of Water: Insights from Quantum Simulations. *J. Phys. Chem. B* **2009**, *113* (17), 5702–5719.  
987 (51) Reddy, S. K.; Moberg, D. R.; Straight, S. C.; Paesani, F. Temperature-dependent vibrational spectra and structure of liquid water from classical and quantum simulations with the MB-pol potential energy function. *J. Chem. Phys.* **2017**, *147*, 244504.  
988 (52) Riera, M.; Gotz, A. W.; Paesani, F. The i-TTM model for ab initio-based ion-water interaction potentials. II. Alkali metal ion-water potential energy functions. *Phys. Chem. Chem. Phys.* **2016**, *18* (44), 30334–30343.  
989 (53) Ceriotti, M.; Fang, W.; Kusalik, P. G.; McKenzie, R. H.; Michaelides, A.; Morales, M. A.; Markland, T. E. Nuclear Quantum Effects in Water and Aqueous Systems: Experiment, Theory, and Current Challenges. *Chem. Rev.* **2016**, *116* (13), 7529–7550.